Collision-time simulation technique for pressure-broadened spectral lines with applications to Ly-α

Gerhard C. Hegerfeldt and Volker Kesting
Institut für Theoretische Physik, Universität Göttingen, D-3400 Göttingen, West Germany
(Received 4 September 1987)

We introduce a new simulation technique which is based on the distribution of the times of collision between plasma particles and a radiating atom. This procedure generates a continuous flow of particles of random velocities and directions through a sphere of interaction around the radiator. It leads to correct statistics while traditional procedures with their reinjection prescriptions are shown to change the statistics. The new technique is applied to a detailed study of Ly-α. The influence of the shielding parameter and the temperature-density dependence are investigated. An asymptotic exponential falloff of the ion dipole autocorrelation function is exhibited, verifying analytic indications. The first *joint* ion-electron simulation of profiles is reported. They agree with the experimental profiles of Grützmacher and Wende.

I. INTRODUCTION

Until the measurements of Kelleher and Wiese[1] and, in particular, those of Grützmacher and Wende,[2] it was accepted in the theory of Stark broadening of spectral lines in a plasma that the ions could be treated as static. The measurements of Ref. 2 of the Ly-α half-width disagreed with contemporary theoretical values[3] by almost a factor of 2. It seems at present that this discrepancy was due to the assumption of static ions.[4] It is difficult to take ion dynamics into account theoretically at a microscopic level, since for ions one has strong overlapping collisions, so that theories using binary collisions, such as the unified theory[5] or the cluster expansions of Ref. 6, cannot be applied. The model microfield method of Brissaud and Frisch[7] was relatively successful in the work of Seidel[8] and Mazure *et al.*[9] in treating ion dynamics. It is, however, a phenomenological approach, not a microscopic theory.

On a microscopic level, important progress has been made by simulation-oriented approaches[10–12] which make possible the evaluation of the analytically unwieldy expressions of the microscopic theory and allow the calculation of line profiles which agree with the experimental profiles to a surprising degree of accuracy. The underlying microscopic model usually treats the plasma particles ("perturbers") as classical quasiparticles which, in the case of neutral radiators, travel on straight paths and whose charge is Debye shielded. Thus the perturbers are regarded as a two-component ideal gas at given density and temperature. In Refs. 10–12 only the ions are simulated, while for the electrons the impact approximation[13] is used. The simulation realizes the model by randomly generating about 125 perturbers[14] in a simulation volume, e.g., a sphere, as in Ref. 11. Since the perturbers are moving, a part of them leaves the sphere during the simulation time, and therefore a perturber-reinjection procedure has to be introduced. This can be done either through periodic boundary conditions in case of a box as simulation volume or as in Ref. 11, whereupon leaving a perturber is reinjected randomly into a surface layer of the sphere with, up to a sign, the same velocity. The sign is chosen so that the perturber moves into the sphere.

Periodic boundary conditions clearly introduce correlations and the improved reinjection method of Ref. 11 is an advance. But also this method introduces correlations and deviations from the behavior of an ideal gas, in a more subtle way though. It can be shown analytically that the reinjection method of Ref. 11 (a) favors large impact parameters and (b) changes the perturber-radiator collision frequency. To exhibit this graphically we have performed a simulation with reinjection method as in Ref. 11 and parameters as in Eq. (4.8). In Fig. 1 the collision frequency $\nu(t)$ is plotted where

$$\nu(t)^{-1}=\langle \tau_2(t)-\tau_1(t)\rangle_{\rm av}\ ,$$

the average time interval between the first and second collision after time t. In an ideal gas the analogous frequency ν_0 is constant. Collision times and their statistics are explained in detail in Sec. II. It is seen that the ratio $\nu(t)/\nu_0$ approaches $\frac{4}{3}$, which is also obtained analytically.

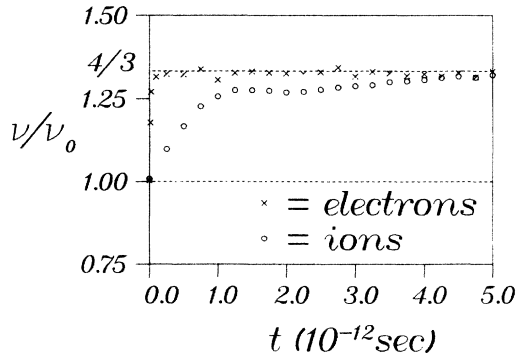

FIG. 1. Collision frequency $\nu(t)$ for reinjection method as in Ref. 11 compared to ideal gas frequency ν_0.

For ions this limit is reached much more slowly than for electrons, in accordance with the square root of their mass ratio. At $t=10^{-12}$ sec the deviation from the correct statistics has become considerable for ions, but for this time the ion dipole autocorrelation function has already dropped to 0.3 (cf. Fig. 3). Therefore, one would hope that this change of statistics will not affect the simulated ion profiles too much. For electrons, however, the deviation from the correct statistics sets in much sooner, so that one would expect a greater effect.

With the above reinjection method, one also has no fluctuations of the particle number in the simulation volume nor of the velocity profile. To avoid all this, it would seem simplest to enlarge the simulation volume sufficiently, the lighter the perturbers, the larger the volume required. There are, however, the following objections.

(i) Computer time rises tremendously.

(ii) It is uneconomical—there are a growing number of peturbers which do not come physically close enough to the radiator to interact and which are, thus, superfluous for the simulation.

Most appropriate would be a simulation that picks out just those perturbers from the infinite gas which are relevant for the interaction, i.e., which are actually in a sphere of interaction of given radius R during a time for which the dipole autocorrelation function is still (appreciably) nonzero. Just this is achieved by the simulation procedure we are proposing, a *collision-time simulation technique.* This procedure generates random collision times and, for each collision, a random velocity and an impact parameter smaller than R. In this way one generates a *continuous flow of perturbers entering and leaving the interaction volume.* Details are explained in Sec. III.

The new technique is used in Sec. IV in a detailed study of ionic and electronic properties of Ly-α by means of individual ion, and electron simulations, and—to our knowledge, for the first time—*joint ion-electron simulations.* We investigate the influence of the shielding parameter, the density-temperature dependence, and validity of the impact approximation. We exhibit an asymptotic exponential fall off of the dipole autocorrelation function for ions and show agreement of calculated and experimental profiles.

For an average number of 125 perturbers in the interaction sphere, the number N of collision times generated, i.e., the *total* number of perturbers, is typically 600–1200 for ions and 3000–5000 for electrons. In our applications we use 250 perturbers in the interaction sphere, with corresponding total number $N=1000-2000$ for ions and $N=5000-8000$ for electrons. Our algorithm requires more memory than the traditional approach, although this can be reduced by program refinements. On the other hand, our algorithm is easily vectorizable, as opposed to the traditional one, thus allowing large savings in computer time.

II. LINE-BROADENING MODEL AND COLLISION-TIME STATISTICS

The electrons of an atom, with Hamiltonian H_A, experience an additional potential if placed in a gas or plasma of classical point particles. The jth perturber contributes a potential $\varphi_j(t)$ to the atomic Hamiltonian, e.g., a Coulomb or a Debye-Hückel potential in case of a plasma, so that the total Hamiltonian is

$$H(t)=H_A+\sum_j \varphi_j(t) \; . \tag{2.1}$$

We denote by $T_H(t,t_0)$ the corresponding time-development operator and consider an optical transition from an unperturbed atomic energy level E_{in} to E_{fin}. By $\mathcal{H}_{\text{in}}$ and $\mathcal{H}_{\text{fin}}$ we denote the associated eigenspaces, with orthonormal bases $\{\,|\,i\,\rangle\}$ and $\{\,|\,f\,\rangle\}$, say. We define

$$\begin{aligned} \omega_0 &:= (E_{\text{in}}-E_{\text{fin}})/\hbar \; , \\ \mathbf{d} &:= -e\mathbf{X} \; , \end{aligned} \tag{2.2}$$

the unperturbed transition frequency and dipole operator, respectively. For simplicity we consider a single radiating electron only. Semiclassical radiation theory gives for the normalized line-shape function $L(\omega)$ for an atom at rest,[13]

$$L(\omega)=(2\pi)^{-1}A\int dt\, e^{i\omega t}\sum_{i,f,i',f'}\langle\langle i\,|\,\mathbf{d}\,|\,f\rangle\langle f\,|\,T_H(t,0)^*\,|\,f'\rangle\langle f'\,|\,\mathbf{d}\,|\,i'\rangle\langle i'\,|\,T_H(t,0)\,|\,i\rangle\rangle_{\text{av}} \; , \tag{2.3}$$

where A is a normalization constant,

$$A^{-1}=\sum_{i,f}|\langle i\,|\,\mathbf{d}\,|\,f\rangle|^2 \; ,$$

and where $\langle\;\rangle_{\text{av}}$ denotes averaging over the perturber configurations. Following Baranger[15] we define the line space

$$\mathcal{H} := \mathcal{H}_{\text{in}}\otimes\mathcal{H}_{\text{fin}} \tag{2.4}$$

and operators $\Phi_j(t)$, $V(t)$, $U(t,t_0)$, and D in $\mathcal{H}$ by

$$\langle if \mid \Phi_j(t) \mid i'f' \rangle := \langle i \mid \varphi_j(t) \mid i' \rangle \delta_{ff'} - \delta_{ii'} \langle f' \mid \varphi_j(t) \mid f \rangle ,$$
$$V(t) := \sum_j \Phi_j(t) ,$$
$$\langle if \mid U(t,t_0) \mid i'f' \rangle := \langle i \mid T_H(t,t_0) \mid i' \rangle \langle f' \mid T_H(t,t_0)^* \mid f \rangle e^{i\omega_0(t-t_0)} , \tag{2.5}$$
$$\langle if \mid D \mid i'f' \rangle := A \langle i \mid \mathbf{d} \mid f \rangle \langle f' \mid \mathbf{d} \mid i' \rangle .$$

The *centered* line profile $I(\Delta\omega)$ is then given by the Fourier transform of the dipole autocorrelation function $C(t)$,

$$C(t) := \mathrm{Tr} \langle DU(t,0) \rangle_{\mathrm{av}} ,$$
$$I(\Delta\omega) := L(\omega_0 + \Delta\omega) = (2\pi)^{-1} \int dt\, e^{i\Delta\omega t} C(t) . \tag{2.6}$$

Note that although the definitions in Eqs. (2.5) are basis dependent the final expression for $I(\Delta\omega)$ is not. We also note that $V(t_1)$ and $V(t_2)$ will, in general, not commute for $t_1 \neq t_2$. With the usual nonquenching assumption one may approximate $\langle i \mid \varphi_j \mid f \rangle$ by 0, thus neglecting transitions caused by the perturbers. Then one shows by a simple calculation

$$\dot{U}(t,t_0) = -\frac{i}{\hbar} V(t) U(t,t_0) . \tag{2.7}$$

This is a stochastic differential equation of Schrödinger-type whose averaged solution has to be Fourier transformed.

Collision-time statistics. The plasma of ions and electrons is treated in the quasiparticle picture as an infinite ideal gas, with charge shielding, for example, in the form of a Debye-Hückel potential. Then the jth perturber, with charge q_j and position $\mathbf{r}_j(t)$, contributes to H in Eq. (2.1),

$$\varphi_j(t) = -eq_j(4\pi\epsilon_0)^{-1} \mid \mathbf{x} - \mathbf{r}_j(t) \mid^{-1} \times \exp[-\xi \mid \mathbf{x} - \mathbf{r}_j(t) \mid / r_D] , \tag{2.8}$$

where $r_D = (\epsilon_0 kT/ne^2)^{1/2}$ is the Debye radius and where ξ is a further shielding parameter which is often, but not always, chosen as 1. Each perturber moves on a straight path,

$$\mathbf{r}_j(t) = \mathbf{x}_j + \mathbf{v}_j t . \tag{2.9}$$

The positions at time 0, $\mathbf{x}_j$ are uniformly distributed and the velocities have a Maxwellian distribution. An equivalent description is in terms of the collision time τ_j—the time of closest approach to the atom located at the origin—and of the impact parameter $\rho_j := \mathbf{r}_j(\tau_j)$ as well as the velocity $\mathbf{v}_j$,

$$\mathbf{r}_j(t) = \boldsymbol{\rho}_j + \mathbf{v}_j(t - \tau_j) . \tag{2.10}$$

In order to have a finite collision rate one has to choose a finite radius R and count only those collisions which have an impact parameter less than R. In an infinite gas there are, without this restriction, infinitely many collisions in any finite time interval. In theoretical considerations one may eventually let R tend to infinity. In our simulation procedure we choose R large enough for the Debye-Hückel potential to have dropped close to zero, as discussed in Sec. III.

The collision times are uniformly distributed and independent of $\boldsymbol{\rho}_j$ and $\mathbf{v}_j$. Of course, $\boldsymbol{\rho}_j$ and $\mathbf{v}_j$ satisfy $\boldsymbol{\rho}_j \perp \mathbf{v}_j$, but otherwise they are independent. The charge q_j is also independent of the other variables. Thus $\Phi_j(t)$, a one-perturber contribution to the potential in line space, is of the form

$$\Phi_j(t) = \Phi(t - \tau_j; \mathbf{v}_j, \boldsymbol{\rho}_j, \mathbf{q}_j) . \tag{2.11}$$

Except for the additional variables $\mathbf{v}_j$, $\boldsymbol{\rho}_j$, and q_j this is similar to shot noise; particles arrive at random, uniformly distributed in time, and each contributing $\Phi(t - \tau_j)$ to the "current," in our case to the matrix-valued potential $V(t)$. This approach with collision-time statistics has been used previously in analytic investigations.[6,16]

Mathematically, the number of particles colliding in $[t_0, t]$ is a Poisson process. In each configuration one can index the perturbers according to their collision times: the nth perturber in this numbering would be the one which collides as the nth after some time t_0 (for perturbers colliding before t_0 one can use $n \leq 0$ [Ref. 16(b)]). The time duration u_n between the nth and $(n+1)$th collision is called the intercollision time. It is exponentially distributed, and different u_n's, for $n > 0$, are independent. This may be used for a mathematical description. For the simulation we proceed slightly differently, as explained below.

III. COLLISION-TIME SIMULATION TECHNIQUE

The underlying idea of our approach becomes particularly transparent for charge shielding by a cutoff at the Debye radius r_D. Then only those perturbers in the infinite gas contribute to $V(t)$ whose impact parameter ρ is smaller than r_D and the other perturbers can be ignored. In the simulation this is achieved by generating collision times $\{\tau_j\}$ and for each τ_j a random velocity $\mathbf{v}_j$ and an impact parameter $\boldsymbol{\rho}_j \perp \mathbf{v}_j$ with $\rho_j \leq r_D$. In this way, only relevant perturbers enter the simulation and one generates a continuous flow of perturbers impinging on the Debye sphere of the radiator from all directions.

Physically—and also numerically—it is better to have charge shielding in terms of a smooth Debye-Hückel potential. Since this rapidly goes to zero for increasing distance, only perturbers with impact parameters of less than a few r_D produce relevant contributions to the total potential $V(t)$. For example, for $\xi = 1$, the field strength at the origin of a perturber at $r_j = 3r_D$ is only 0.03 of the field strength of a perturber at $r_j = r_D$. We therefore

choose a sphere of radius R such that the perturbers outside can be safely ignored. A good value is $R \approx 3r_D$. Then the same simulation procedure as before can be applied, but now with impact parameters $\rho_j \leq R$.

One has to calculate the Fourier transform of the dipole autocorrelation function

$$C(t)=\mathrm{Tr}[\langle DU(t,0)\rangle_{\mathrm{av}}] \tag{3.1}$$

and one therefore has to know it for sufficiently large times. In our applications we have the symmetry

$$C(-t)=C(t) , \tag{3.2}$$

so that numerically one needs $C(t)$ only in a time interval $[0,T]$ where, for $t \geq T$, $C(t)$ has become sufficiently small. Since, conversely, $C(t)$ is essentially the inverse Fourier transform of $I(\Delta\omega)$ by Eq. (2.6), one can roughly estimate from the experimental linewidth how broad $C(t)$ is and how large T has to be chosen. In our application to Ly-α we find that $C(t)$ asymptotically falls off exponentially also for ions, which verifies analytic indications.[16(b),16(c)] The onset of the exponential behavior is used to determine a lower bound for T and to continue $C(t)$ for larger t.

Once the time interval $[0,T]$ is chosen one has to decide how many collision times to generate. Now, slow perturbers may collide well before $t=0$ and still be in the interaction volume at times later than $t=0$. Therefore one has to generate collision times in an interval $[-\Delta, T+\Delta]$, where Δ is a "thermalization time." For more massive—and thus slower—perturbers, Δ has to be larger than for lighter perturbers (cf. Fig. 2). For $R \approx 3r_D$, a good value for Δ is, in terms of the plasma frequency $\omega_p=(ne2/\epsilon_0 m)^{1/2}$,

$$\Delta = 10\omega_p^{-1} . \tag{3.3}$$

One can show analytically that with this value of Δ, on the average, only one perturber in 1000 with collision time outside $[0,T]$ is missed by the simulation.

To generate the random-collision times in $[-\Delta, T+\Delta]$ there are two essentially equivalent ways. One is to generate *exponentially* distributed intercollision times u_n and, starting at $t_0=-\Delta$, to add them up to give collision times τ_n',

$$\tau_n' = t_0 + \sum_0^{n-1} u_\alpha , \tag{3.4}$$

where $u_0=\tau_1-t_0$. This is stopped when $\tau_n' \geq T+2\Delta$.

We use the following alternative way. Let ν_R be the mean collision frequency of a perturber species, ions, say, with respect to a given radius R,

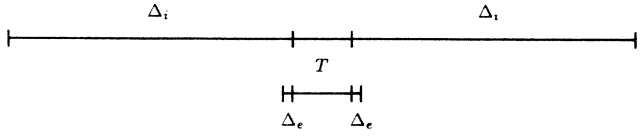

FIG. 2. Schematic comparison of thermalization times Δ_i and Δ_e for ions and electrons.

$$\nu_R = \sqrt{4\pi} R^2 n v_0 , \tag{3.5}$$

where $v_0=(2kT/m)^{1/2}$. The mean number of collisions in $[-\Delta, T+\Delta]$ is then $\nu_R(T+2\Delta)$. One may therefore generate

$$N=[\nu_R(T+2\Delta)+\tfrac{1}{2}] \tag{3.6}$$

random collision times $\tau_1, \ldots, \tau_N$ *uniformly* distributed on $[-\Delta, T+\Delta]$. This is numerically easier to handle than the exponential distribution. In this approach the number N is fixed, while in the former the total perturber number fluctuates. However, if the time interval and, thus, N are large enough, this makes no essential difference. In either approach, though, the number of perturbers colliding in $[0,T]$ fluctuates with the configuration, and in each configuration the instantaneous perturber number in the sphere and the perturber velocities fluctuate with time. Although $\Delta_i \gg \Delta_e$ one has $N_i < N_e$. In our applications, we have typically $N_i \approx 1000-2000$ for ions and $N_e \approx 5000-8000$ for electrons. In addition, because the ions are much slower than the electrons, their potential is easier to handle. Therefore the computer time needed for ion simulations is far less than for electrons.

Summarizing, our simulation procedure for a single-perturber species, in principle, runs as follows. One chooses the radius R of the interaction sphere, $R \approx 3r_D$, and determines the collision frequency ν_R from Eq. (3.5) and N from Eq. (3.6). Then one generates N random collision times $\tau_1, \ldots, \tau_N$ uniformly distributed in $[-\Delta, T+\Delta]$, where $\Delta \approx 10\omega_p^{-1}$. For each collision time τ_j one generates a random velocity $\mathbf{v}_j$, as follows. In polar coordinates we write

$$v_j = v_j \begin{pmatrix} \sin\vartheta_j & \cos\varphi_j \\ \sin\vartheta_j & \sin\varphi_j \\ \cos\vartheta_j & \end{pmatrix} . \tag{3.7}$$

Then φ_j is uniformly distributed on $[0,2\pi]$ and ϑ_j has density $\frac{1}{2}\sin\vartheta_j$ on $[0,\pi]$. The density for v_j is given by the modified Maxwell distribution

$$2\frac{v^3}{v_0^4}\exp(-v^2/v_0^2) . \tag{3.8}$$

The extra factor of v comes from the correct change of variables from $(\mathbf{x}_j(0), \mathbf{v}_j)$ to $(\tau_j, v_j, \vartheta_j, \varphi_j, \boldsymbol{\rho}_j)$. After $\mathbf{v}_j$ one generates a random impact parameter $\boldsymbol{\rho}_j$, which is uniformly distributed on a disk of radius R perpendicular to $\mathbf{v}_j$. Since $\boldsymbol{\rho}_j \perp \mathbf{v}_j$ we can write with the unit vectors $\mathbf{e}_{\vartheta_j}$ and $\mathbf{e}_{\varphi_j}$ in the ϑ and φ directions of the polar coordinates in Eq. (3.7),

$$\boldsymbol{\rho}_j = \rho_j \cos\psi_j \mathbf{e}_{\vartheta_j} + \rho_j \sin\psi_j \mathbf{e}_{\varphi_j} . \tag{3.9}$$

Then ψ_j is uniformly distributed on $[0,2\pi]$ and ρ_j has the density $2\rho/R^2$ on $[0,R]$. Now one calculates $V(t)$ from Eqs. (2.5) and numerically determines $U(t,0)$ from Eq. (2.7). Averaging over a larger number N_c of configurations, one obtains $\langle U(t,0)\rangle_{\mathrm{av}}$ and then $I(\Delta\omega)$

by Fourier transformation.

For a joint simulation of two perturber species, ions and electrons, one has two different time scales given by the respective plasma frequencies, $\omega_{p,i}$ and $\omega_{p,e}$. In this case we choose two Δ's, $\Delta_i \approx 10\omega_{p,i}^{-1}$ and $\Delta_e \approx 10\omega_{p,e}^{-1}$, determine the collision frequencies $\nu_{R,i}$ and $\nu_{R,e}$ from Eq. (3.5), and the corresponding N_i and N_e from Eq. (3.6). Then we generate N_i and N_e random-collision times in $[-\Delta_i, T+\Delta_i]$ and $[-\Delta_e, T+\Delta_e]$, respectively, and for each a random velocity and perpendicular impact parameter. The velocities are distributed with the respective mass parameter. As before, we calculate

$$V(t)=V_i(t)+V_e(t) ,$$

solve Eq. (2.7) numerically for those quantities needed to determine $C(t)$, and Fourier transform.

IV. APPLICATION TO Ly-α

We have performed simulations for different perturber species: (i) ion simulations, (ii) electron simulations, and (iii) joint ion-electron simulations.

Since we are interested in the line center and not in asymmetry of the wings we are using the customary dipole approximation for the Debye-Hückel potential in Eq. (2.8). The monopole term just causes a common shift of all energy levels and drops out in Eqs. (2.5). The dipole approximation gives the symmetry $C(-t)=C(t)$ in Eq. (3.2) by the reflection invariance of the distribution of $[\mathbf{x}_j(0)]$, and from this the symmetry of the line follows. In this approximation, a single perturber contributes to the Hamiltonian H,

$$\varphi_j(t)=-\mathbf{d}\cdot\mathbf{E}^{(j)}(t) , \tag{4.1}$$

where $\mathbf{E}^{(j)}$ is the electric field of the perturber at the origin,

$$\mathbf{E}^{(j)}(t)=-q_j\frac{\mathbf{r}_j(t)}{r_j(t)^3}[1+\xi r_j(t)/r_D] \times \exp[-\xi r_j(t)/r_D] . \tag{4.2}$$

If we define $\tilde{\mathbf{d}}$ in line space by

$$\langle if \mid \tilde{\mathbf{d}} \mid i'f' \rangle := \langle i \mid \mathbf{d} \mid i' \rangle \delta_{ff'} - \delta_{ii'} \langle f' \mid \mathbf{d} \mid f \rangle , \tag{4.3}$$

the potential $V(t)$ becomes

$$V(t)=-\tilde{\mathbf{d}}\cdot\sum_j \mathbf{E}^{(j)}(t) \equiv -\tilde{\mathbf{d}}\cdot\mathbf{E}(t) , \tag{4.4}$$

where $\mathbf{E}(t)$ is the microfield at the origin.

As in Ref. 11 we take the radiator at rest, employ as effective mass of the perturbers the reduced mass μ of the perturber-radiator system, and then convolute with the Doppler profile.[17] In the case of a pure ion simulation we convolute the ion profile with an electron profile obtained by the impact approximation and with the Doppler profile.

Let $\mid nlm \rangle$ be the hydrogen eigenstates. For Lyman lines, $\mathcal{H}_{\text{fin}}$ is one dimensional, spanned by $\mid f \rangle := \mid 100 \rangle$. For Ly-$\alpha$ we take as basis in $\mathcal{H}_{\text{in}}$ the vectors $\mid i \rangle$, $i=0,1,2,3$ given by

$$\mid 200 \rangle, \frac{i}{\sqrt{2}}(\mid 211 \rangle - \mid 21-1 \rangle), \frac{1}{\sqrt{2}}(\mid 211 \rangle + \mid 21-1 \rangle), -i \mid 210 \rangle . \tag{4.5}$$

In the basis $\mid i \rangle \mid f \rangle$, $i=0,1,2,3$ one has, in line space,

$$-\frac{i}{\hbar}V(t)=\frac{i}{\hbar}\tilde{\mathbf{d}}\cdot\mathbf{E}=\frac{3ea_0}{\hbar}\begin{bmatrix} 0 & E_1 & E_2 & E_3 \\ -E_1 & 0 & 0 & 0 \\ -E_2 & 0 & 0 & 0 \\ -E_2 & 0 & 0 & 0 \end{bmatrix} , \tag{4.6}$$

where a_0 is the Bohr radius. Now Eq. (2.7) is a *real* matrix equation. The matrix D has diagonal elements only which are 0 for $l=0$ and $\frac{1}{3}$ for $l=1$. By rotation symmetry, $\langle U(t,0) \rangle_{\text{av}}$ is also diagonal and, in the $l=1$ subspace, a multiple of unity. Therefore, one only needs $\langle f \mid \langle 1 \mid U \mid 1 \rangle \mid f \rangle$, which in view of Eq. (4.6) is obtained by a single system of four coupled real linear differential equations. However, to improve the statistics, we calculate directly,

$$\mathrm{Tr}(DU)=\tfrac{1}{3}\sum_{i=1}^{3}\langle f \mid \langle i \mid U \mid i \rangle \mid f \rangle , \tag{4.7}$$

by the method of Gigosos *et al.*[18] which involves the solution of two systems of four coupled real linear differential equations.

Due to the singularity of the dipole approximation at the origin, we employ, as is customary, a cutoff r_0 for small r. In the collision-time technique this is easily done by allowing impact parameters $\rho_j \geq r_0$ only. We have chosen $r_0=5a_0$. Unless otherwise explicitly stated we have taken the following parameter values:

$$T=16\,000\,\mathrm{K}, \quad N=2\times10^{23}\,\mathrm{m}^{-3} ,$$
$$\Delta_i=1.5\times10^{-11}\,\mathrm{sec}, \quad \Delta_e=5\times10^{-13}\,\mathrm{sec} , \tag{4.8}$$
$$R=(3N_R/4\pi n)^{1/3}, \quad N_R=250 .$$

For μ_i, the reduced mass of the radiator-ion system, we have taken the proton mass, and for μ_e we have taken the electron mass. The number N_c of configurations is, in general, $N_c=5000$ for ion simulations and $N_c=1000$ for electron and joint ion-electron simulations. We now state our results.

A. Exponential falloff of dipole autocorrelation function

There are analytic indications that the dipole autocorrelation function, $C(t)=\mathrm{Tr}[D\langle U(t,0) \rangle_{\text{av}}]$ has an asymptotically exponential falloff [cf. Refs. 16(b) and 16(c)]. We have tested this for ions and electrons with

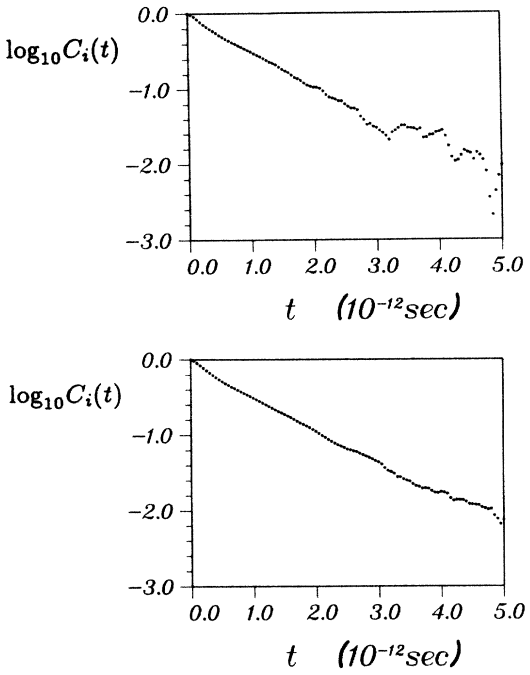

FIG. 3. Exponential falloff of the ion dipole autocorrelation function. Top, $N_c = 1000$; bottom, $N_c = 10\,000$.

different configuration numbers N_c. For ions the results are plotted in Fig. 3. The exponential behavior already sets in at about 0.75×10^{-12} sec. At a later stage this falloff is drowned in noise, depending on the number N_c of configurations. With the onset of noise the simulated $C_i(t)$ may be replaced by its exponential asymptote. This allows a much higher resolution of $I(\Delta\omega)$ by fast Fourier transform. For electrons the results are plotted in Fig. 4. It is seen that the exponential form sets in almost immediately. This verifies the impact approximation for electrons.[19]

B. Influence of the shielding parameter

In Eq. (4.2) ξ determines the falloff of the electric field of a perturber with increasing distance. Most authors take $\xi = 1$, but other values have been used, e.g., $\xi = \sqrt{2}$ in Ref. 20 and $\xi = \sqrt{3/2}$ in Ref. 21. We have performed simulations for ions and for electrons for values of ξ be-

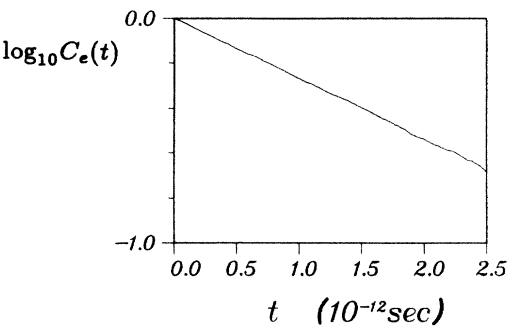

FIG. 4. Exponential falloff of the electron dipole autocorrelation function $N_c = 1000$.

TABLE I. Half-widths for different shielding parameters ξ and simulations of ions (Γ_i), electrons (Γ_e), and convolution of ion simulation with electron impact and Doppler profile (Γ_{tot}).

Γ_{tot} (Å)	Γ_e (Å)	Γ_i (Å)	ξ
0.315	0.108	0.149	0.6
0.312	0.101	0.155	0.8
0.308	0.095	0.160	1.0
0.305	0.090	0.164	1.2
0.300	0.085	0.165	1.4

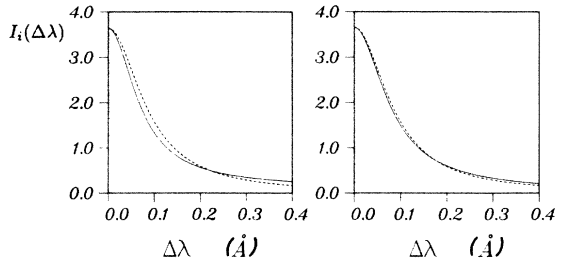

FIG. 5. Increasing Lorentzian character of the ion profile for increasing ξ. Left $\xi = 0.6$, right $\xi = 1.4$. Dashed curve is a Lorentzian with same maximum.

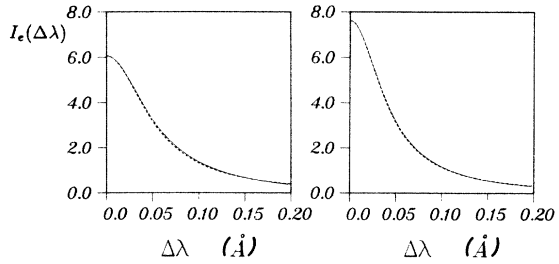

FIG. 6. Electron profiles for $\xi = 0.6$ (left) and $\xi = 1.4$ (right). Dashed curve is a Lorentzian with same maximum.

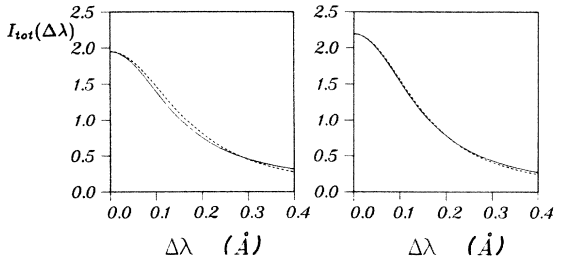

FIG. 7. Complete profiles for $\xi = 0.6$ (left) and $\xi = 1.4$ (right). The impact approximation was used for the electrons. Dashed curve as in Fig. 5.

tween 0.6 and 1.4. The results are collected in Table I and Figs. 5–7.

There is a qualitatively different behavior for ions and electrons. For the former the half-width Γ_i increases for increasing ξ and $I_i(\Delta\omega)$ approaches more and more a Lorentzian. The maximum remains constant, which means that for increasing ξ the line wings are attenuated in comparison to the line center.

For electrons, on the other hand, the profile is essentially Lorentzian for all ξ considered, again verifying the impact approximation. The maximum, however, increases for higher shielding and the half-width decreases correspondingly. As in the case of ions the line wings are again attenuated for increasing ξ, which in view of the decrease of field strength is physically expected.

Convolution of ion and electron profile partially cancels the counteracting effects. The complete profiles in Fig. 7, which include Doppler broadening, retain only relatively weak dependence on ξ.

The increasing Lorentzianness of the ion profile may be understood from the fact that for increasing shielding the collisions show less overlapping and therefore the profile becomes more electronlike.

C. Temperature-density dependence

In this section we have performed ion simulations with $N_c=2000$ for 36 parameter values and have treated the electrons by the impact approximation to keep the central-processing-unit (CPU) time down. The results are collected in Figs. 8–10 and Table II.

The half-width is seen to vary approximately linearly with density both for ions and electrons in the plotted range from $1-2\times10^{23}$ m^{-3}. For the densities $n(10^{23}$ m$^{-3})=1,2,3,4$ and several temperatures, ion and electron simulations were also performed; cf. Table II. For higher densities the ion half-width Γ_i varies markedly slower while the electron half-width Γ_e still varies linearly.

Ions and electrons have opposite temperature dependence in the range of Figs. 8 and 9. Γ_i increases with temperature; Γ_e decreases. Therefore, the temperature dependence of the complete profile is less pronounced. For $n(10^{23}$ m$^{-3})=2$ and $T=12\,000-16\,000$ K, Γ_i increases by about 25%, Γ_e decreases by about 6%, and for the complete profile $\Gamma_{\rm tot}$ increases only by 6%. Since experiments[2(b)] did not show a measurable temperature dependence in this region, these 6% changes may be an artifact of the simulation.

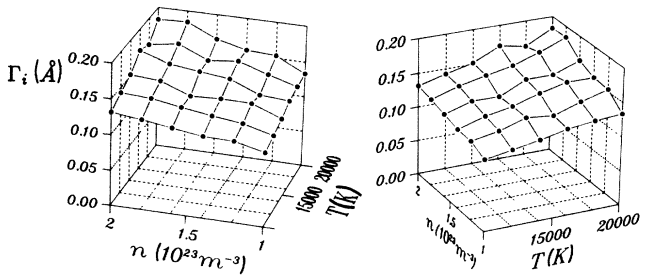

FIG. 8. Temperature-density dependence of half-width for ions.

D. Comparison with experiment

We have calculated profiles and half-widths for the experimental parameter values of Grützmacher and Wende.[2] In Ref. 2(a) complete half-widths are given, while in Ref. 2(b) reduced profiles are displayed which are obtained from the experimental profiles by deconvolution of the Doppler profile. In Table III we compare various experimental half-widths (in parentheses the associated reduced half-widths) with Γ_{ie} obtained from joint ion-electron simulations and Γ_{i*e} from ion simulations convoluted with electron impact profiles. We also give the old theoretical values[22] for which the ions were treated as static. The simulation agrees well with experiment.

In Figs. 11–14 reduced profiles are shown, both for joint ion-electron simulations and for simulated ion profiles convoluted with electron impact profiles. The dots are experimental values. At small densities the values of the joint ion-electron simulations start out to be slightly higher than the experimental ones, then they decrease relatively, agree for $n=3\times10^{23}$ m^{-3} and end up slightly lower for $n=4\times10^{23}$ m^{-3}.

The convolutions of simulated ion profiles and electron impact profiles have a lower maximum than the jointly simulated ones, although for the highest density the difference is very small. This seems to indicate that in the factorization $C(t)=C_i(t)C_e(t)$ of the dipole autocorrelation function, the neglect of correlations introduces a small error. In Ref. 2(b) the experimental uncertainties are given as 6%; for the simulated profiles we estimate them to be about 5%.

V. CONCLUSION AND OUTLOOK

We have presented a new simulation technique based on collision times which, in contrast to traditional pro-

TABLE II. Half-widths for various temperatures and densities.

Γ_e (impact approximation)	Γ_e (simulation)	Γ_i (simulation)	T (10^3 K)	n (10^{23} m^{-3})
0.054	0.055	0.115	12.7	1
0.096	0.097	0.155	13.2	2
0.135	0.134	0.172	13.2	3
0.170	0.173	0.195	14.0	4

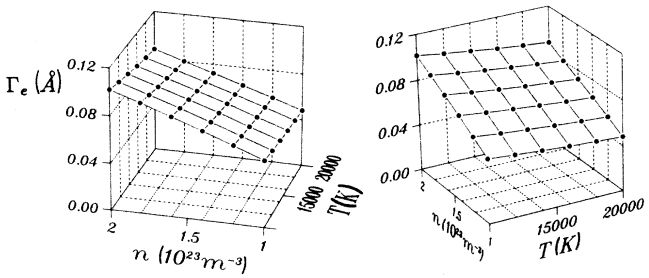

FIG. 9. Temperature-density dependence of half-width for electrons (impact approximation).

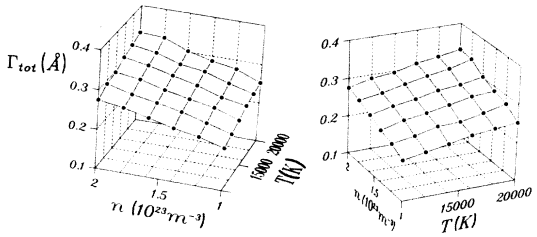

FIG. 10. Temperature-density dependence of half-width of the complete profile obtained by convolution of the ion profile, the electron impact profile, and the Doppler profile.

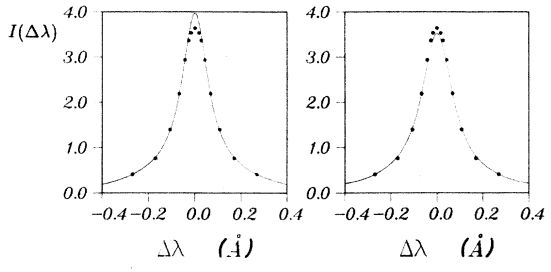

FIG. 11. Reduced Ly-α profiles for $T=12\,700$ K, $n=1\times10^{23}$ m^{-3}. Joint ion-electron simulation (left) and ion simulation convoluted with electron impact profile (right). Dots are experimental values for an Ar^+ plasma [Ref. 2(b)].

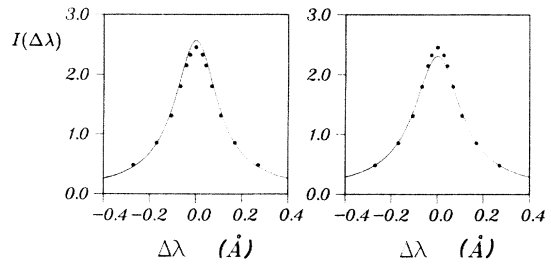

FIG. 12. Profiles as in Fig. 11: $T=13\,200$ K, $n=2\times10^{23}$ m^{-3}.

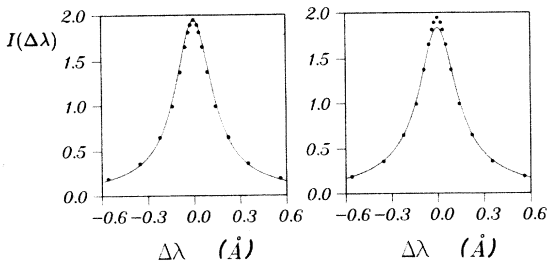

FIG. 13. Profiles as in Fig. 11: $T=13\,200$ K, $n=3\times10^{23}$ m^{-3}.

cedures, leads to correct statistics for fast perturbers also, in particular, for electrons. We have demonstrated the versatility of our method by various applications to Stark broadening of Ly-α and have performed, to our knowledge, the first joint ion-electron simulations reported so far. We have exhibited an asymptotic exponential falloff of the ion dipole autocorrelation function, verifying analytic indications. For electrons this exponential behavior sets in much sooner, which verifies the impact approximation. We have studied the behavior under variation of the shielding parameter ξ and have found a tendency towards a more Lorentzian character of the profile for increasing ξ. The temperature-density dependence of half-widths has been investigated and displayed graphically. For the profiles measured by Grützmacher and Wende we have calculated the corresponding profiles by our simulation technique. They agree with the experimental ones.

Our simulation technique can be extended to ionic radiators for which the classical trajectories are hyperbolas rather than straight lines. These trajectories can be described by means of pseudocollision times corresponding to the incoming asymptotes of the hyperbolas.

Throughout we have used the dipole approximation for the electric microfield, and due to its singularity at the origin we have introduced a customary cutoff for small impact parameters. This is avoidable if one uses the complete Debye-Hückel potential as in Ref. 6(b), since then there is no singularity. In this way one could also perform simulation studies of the red-blue asymmetry of the profiles.

Doppler broadening was taken into account by the usual convolution procedure[17] with effective perturber masses given by the reduced masses of the radiator-

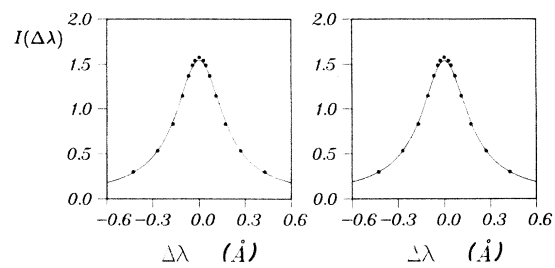

FIG. 14. Profiles as in Fig. 11: $T=14\,000$ K, $n=4\times10^{23}$ m^{-3}.

TABLE III. Half-widths for four temperature-density values (in parentheses, reduced half-widths). Γ_{expt}, experiment; Γ_{ie} joint ion-electron simulation; Γ_{i*e} ion simulation, impact approximation for electrons. The theoretical values are taken from Ref. 22.

Γ_{theory} (Å)	Γ_{i*e} (Å)	Γ_{ie} (Å)	Γ_{expt} (Å)	T (10^3 K)	n (10^{23} m^{-3})
0.14 (0.05)	0.23 (0.17)	0.21 (0.15)	0.23 (0.17)	12.7	1
0.16 (0.09)	0.30 (0.26)	0.28 (0.23)	0.30 (0.24)	13.2	2
0.29 (0.13)	0.36 (0.32)	0.34 (0.31)	0.36 (0.29)	13.2	3
0.22 (0.16)	0.41 (0.38)	0.41 (0.39)	0.42 (0.37)	14.0	4

perturber systems. Though very successful, this procedure is theoretically not quite satisfactory, since in principle there may be correlations between both broadening mechanisms. Our simulation technique can be applied also in the more realistic situation in which the radiating atoms are not at rest but moving, too. If one uses the correct expression for $I(\Delta\omega)$ with moving radiators this will also take Doppler broadening into account. Such a joint ion-electron-radiator simulation is presently under way.

ACKNOWLEDGMENT

The numerical calculations were performed on the Cray Research X-MP/24 computer of the Konrad-Zuse-Zentrum für Informationstechnik, Berlin.

[1]D. E. Kelleher and W. L. Wiese, Phys. Rev. Lett. **31**, 1431 (1973).

[2](a) K. Grützmacher and B. Wende, Phys. Rev. A **16**, 243 (1977); **18**, 2140 (1978); (b) K. Grützmacher, dissertation, University of Berlin, 1979 (unpublished).

[3]C. R. Vidal, J. Cooper, and E. W. Smith, Astrophys. J. Suppl. Ser. **25**, 37 (1973).

[4]R. W. Lee, J. Phys. B **12**, 1145 (1979); H. R. Griem, Phys. Rev. A **20**, 606 (1979); D. Voslamber and R. Stamm, in *Spectral Line Shapes,* edited by B. Wende (de Gruyter, Berlin, 1981), p. 63.

[5]D. Voslamber, Z. Naturforsch. Teil A **24**, 1458 (1969); E. W. Smith, J. Cooper, and C. R. Vidal, Phys. Rev. **185**, 140 (1969).

[6](a) W. von Waldenfels, in *Probability and Information Theory II,* Vol. 296 of *Lecture Notes in Mathematics,* edited by M. Behara *et al.* (Springer, Berlin, 1973), p. 19; (b) G. C. Hegerfeldt and R. Reibold, Z. Naturforsch. Teil A **37**, 305 (1982).

[7]A. Brissaud and U. Frisch, J. Quant. Spectrosc. Radiat. Transfer **11**, 1767 (1971).

[8]J. Seidel, Z. Naturforsch. Teil A **32**, 1207 (1977); **35**, 679 (1980).

[9]A Mazure, C. Goldbach, and G. Nollez, Ann. Phys. (Paris) **5**, 219 (1980).

[10](a) R. Stamm and D. Voslamber, J. Quant. Spectrosc. Radiat. Transfer **22**, 599 (1979); (b) R. Stamm, in *Spectral Line Shapes,* edited by K. Burnett (de Gruyter, Berlin, 1983), Vol. 2, p. 3.

[11](a) R. Stamm and E. Smith, Phys. Rev. A **30**, 450 (1984); R. Stamm, E. W. Smith, and B. Talin, *ibid.* **30**, 2039 (1984); (b) R. Stamm, Y. Botzanowski, V. P. Kaftandjian, B. Talin, and E. W. Smith, Phys. Rev. Lett. **52**, 2217 (1984); (c) R. Stamm and B. Talin, Ann. Phys. (Paris) **9**, 687 (1984).

[12]J. Seidel, Phys. Rev. Lett. **57**, 2154 (1986); Ann. Phys. (Paris), Suppl. No. (3) **11** (3), 149 (1986).

[13]Compare, e.g., H. R. Griem, *Spectral Line Broadening by Plasmas* (Academic, New York, 1974).

[14]Only 40 perturbers were taken in a pure electron simulation by M. A. Gigosos, V. Cardeñoso, and F. Torres, J. Phys. B **19**, 3027 (1986).

[15]M. Baranger, Phys. Rev. **111**, 494 (1958).

[16](a) G. C. Hegerfeldt and R. Reibold, Phys. Lett. **82A**, 340 (1981); (b) J. Stat. Phys. **32**, 313 (1983); **32**, 337 (1983); (c) H. Schulze, dissertation, University of Göttingen, 1987 (unpublished).

[17]J. Seidel, Z. Naturforsch. Teil A **34**, 1385 (1979); J. Seidel and R. Stamm, J. Quant. Spectrosc. Radiat. Transfer **27**, 499 (1982).

[18]M. A. Gigosos, J. Fraile, and F. Torres, Phys. Rev. A **31**, 3509 (1985).

[19]Compare also Ref. 14.

[20]B. Mozer and M. Baranger, Phys. Rev. **118**, 626 (1960); see Ref. 10(a).

[21]G. H. Ecker and A. Schumacher, Z. Naturforsch. Teil A **30**, 413 (1975); see Ref. 11(b).

[22]In Ref. 3, quoted from Ref. 2(b).